

# 1 Lancet: genome-wide somatic variant calling 2 using localized colored DeBruijn graphs

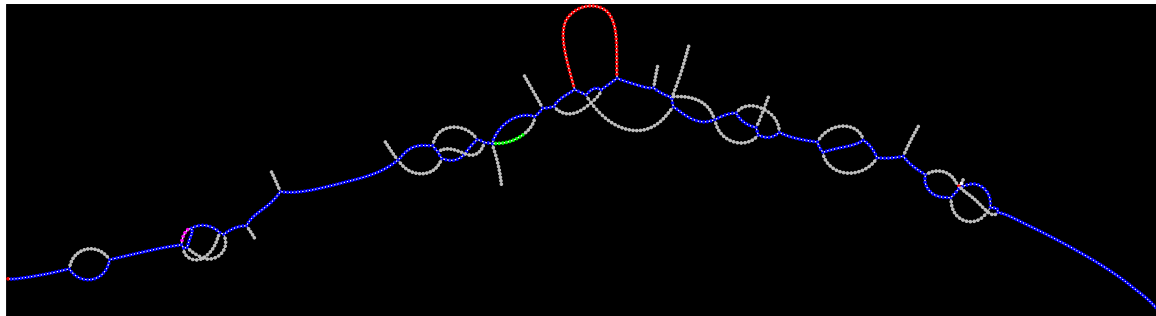
3 Giuseppe Narzisi<sup>1</sup>, André Corvelo<sup>1</sup>, Kanika Arora<sup>1</sup>, Ewa A. Bergmann<sup>1,\*</sup>, Minita Shah<sup>1</sup>, Rajeeva  
4 Musunuri<sup>1</sup>, Anne-Katrin Emde<sup>1</sup>, Nicolas Robine<sup>1</sup>, Vladimir Vacic<sup>1,†</sup>, Michael C. Zody<sup>1</sup>

5  
6 <sup>1</sup> New York Genome Center, New York, USA.  
7 \* Present address: Illumina Cambridge Ltd, Little Chesterford, United Kingdom.  
8 † Present address: 23andMe, Inc., Mountain View, CA, USA.

9 Corresponding author: G.N. ([gnarzisi@nygenome.org](mailto:gnarzisi@nygenome.org))

10 **Reliable detection of somatic variations is of critical importance in cancer research. Lancet is**  
11 **an accurate and sensitive somatic variant caller which detects SNVs and indels by jointly**  
12 **analyzing reads from tumor and matched normal samples using colored DeBruijn graphs.**  
13 **Extensive experimental comparison on synthetic and real whole-genome sequencing datasets**  
14 **demonstrates that Lancet has better accuracy, especially for indel detection, than widely used**  
15 **somatic callers, such as MuTect, MuTect2, LoFreq, Strelka, and Strelka2. Lancet features a**  
16 **reliable variant scoring system which is essential for variant prioritization and detects low**  
17 **frequency mutations without sacrificing the sensitivity to call longer insertions and deletions**  
18 **empowered by the local assembly engine. In addition to genome-wide analysis, Lancet allows**  
19 **inspection of somatic variants in graph space, which augments the traditional read alignment**  
20 **visualization to help confirm a variant of interest. Lancet is available as an open-source**  
21 **program at <https://github.com/nygenome/lancet>.**

22 Reliable detection of somatic variants from next-generation sequencing data requires the ability to  
23 effectively handle a broad range of diverse conditions such as aneuploidy, clonality, and purity of  
24 the input tumor material. The sensitivity and specificity of any somatic mutation calling approach  
25 varies along the genome due to differences in sequencing read depths, error rates, mutation types  
26 and their sizes (e.g., SNVs, indels, CNVs). Micro-assembly approaches<sup>1</sup> have been successful at  
27 calling indels up to a few hundred base pairs in length, allowing inquiry into the twilight zone  
28 between longer indels and shorter CNVs. However, existing micro-assembly methods rely on  
29 separate assembly of tumor and matched normal data, which has limitations in regions with low  
30 supporting coverage, repeats, and large indels. Accounting for these variables requires flexible  
31 methods that can adapt to the specific context of each genomic region.



32

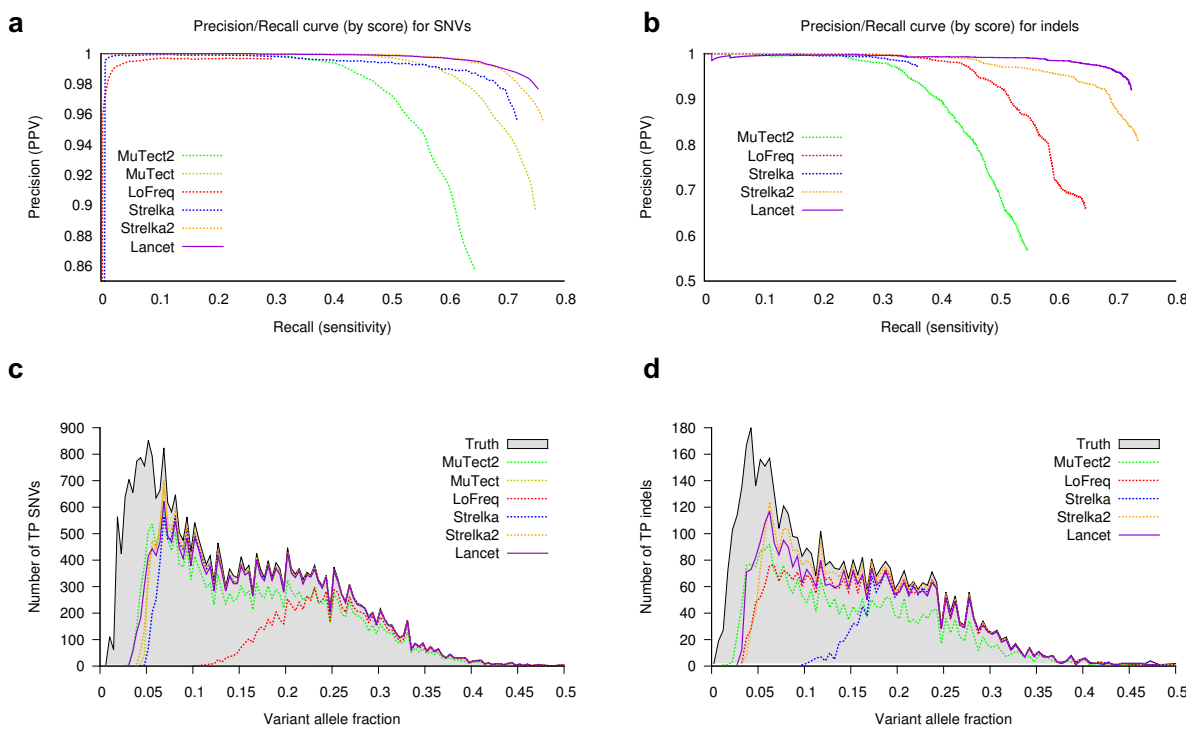
33 **Figure 1. Colored DeBruijn illustration.** Example of colored DeBruijn graph rendered using Lancet for a short  
34 region of 400bp containing an insertion. Blue nodes correspond to  $k$ -mers shared by both the tumor and the normal  
35 samples, red nodes correspond to  $k$ -mers private to the tumor, green nodes correspond to  $k$ -mers private to the normal,  
36 and white nodes correspond to low coverage  $k$ -mers due to sequencing errors.

37 We here introduce a new somatic SNV and indel caller, *Lancet*, which uses localized colored  
38 DeBruijn graphs (**Fig. 1**) to detect somatic variants with high accuracy in paired tumor and normal  
39 samples. Lancet builds upon the effective assembly engine we introduced in the Scalpel<sup>2</sup> variant  
40 caller, that localizes the assembly to small genomic regions. However, unlike Scalpel, Lancet  
41 jointly assembles reads from a tumor and a matched normal sample into colored DeBruijn graphs  
42 that are automatically optimized according to the repeat composition of each sequence  
43 (**Supplementary Fig. 1** and **Online Methods**). The colored DeBruijn graph assembly paradigm  
44 was initially introduced and applied to detection and genotyping of both simple and complex  
45 germline variants in a single individual or population<sup>3</sup>. We here demonstrate that this paradigm is  
46 even more powerful in the context of somatic variant detection. Unlike the initial work of Iqbal *et*  
47 *al.*, where the colored DeBruijn graph is constructed for the whole genome, Lancet builds a local  
48 colored DeBruijn graph in a short genomic region (default 600bp) following the micro-assembly  
49 paradigm<sup>1, 2</sup>. The local assembly paradigm makes a very detailed analysis of the graph structure  
50 computationally tractable, allowing the detection of low frequency mutations private to the tumor  
51 without sacrificing the sensitivity to call longer mutations. In the Lancet framework, somatic  
52 variants correspond to simple paths in the graph whose nodes ( $k$ -mers) belong only to the tumor.  
53 Partially supported variants in the normal sample can be easily detected and classified as germline  
54 variants (**Supplementary Fig. 2**). Among its many features, Lancet employs: 1) an Edmonds–Karp  
55 style network-flow algorithm to efficiently enumerate all haplotypes in a genomic region; 2) on-  
56 the-fly short tandem repeat (STR) analysis of the sequence context around each variant; 3) a highly  
57 reliable scoring system; 4) carefully tuned filters to prioritize higher confidence somatic variants;  
58 and 5) a simple and efficient active region module to skip the analysis of genomic regions with no  
59 evidence of variation (**Online Methods**). Finally, in addition to running the tool in discovery  
60 mode, Lancet can be used interactively for an in-depth analysis of a region of interest, similarly to  
61 other bioinformatics utilities used for operating on BAM files, such as samtools<sup>4</sup>, bamtools<sup>5</sup>,  
62 bedtools<sup>6</sup>, etc. Colored DeBruijn graphs can be easily exported and rendered to visualize variants

63 of interest in graph space (**Fig. 1**), which can help in confirming a variant. This feature  
64 complements read alignment visualization tools such as the Integrative Genomics Viewer (IGV)<sup>7</sup>  
65 and provides another useful view into the data that supports variant calling.

## 66 Results

67 We performed extensive experimental comparisons using several synthetic and real-world datasets  
68 designed to assess the variant calling abilities of Lancet under diverse tumor clonality/cellularity  
69 and sequencing conditions on a range of Illumina platforms (HiSeq 2000, HiSeq 2500, HiSeq X)  
70 commonly used for whole-genome sequencing. We compared Lancet to some of the most widely  
71 used somatic variant callers, including MuTect<sup>8</sup>, MuTect2, LoFreq<sup>9</sup>, Strelka<sup>10</sup>, and Strelka2<sup>11</sup>.  
72 Benchmarking datasets include (1) virtual tumors generated from real germline sequencing reads,  
73 that contain a predefined list of somatic mutations with known variant allele fractions (VAF); (2)  
74 synthetic tumors from the ICGC-TCGA DREAM mutation calling challenge<sup>12</sup>; (3) matched tumor  
75 and normal from a medulloblastoma case from the ICGC PedBrain Tumor project<sup>13</sup>; and (4) real  
76 data from a highly genetically concordant pair of primary and metastatic cancer lesions<sup>14</sup>.



77 **Figure 2. Performance of Lancet and other methods on the virtual tumors.** (a) Precision/recall curves for somatic  
78 SNVs called by Lancet, MuTect, MuTect2, LoFreq, Strelka, and Strelka2 on the virtual tumor. Curves are generated by  
79 sorting the variants based on the confidence or quality score (QUAL) assigned by each tool. Each point on the curve  
80 corresponds to precision and recall of all the SNVs with confidence score less or equal to a specific quality threshold.  
81 The curve for an ideal tool (with no errors) should start from the top left corner (with precision=1) and produce a  
82 straight horizontal line. Any deviation from a straight line is due to errors introduced by the variant calling process.  
83

84 Specifically, deviations at low recall rates are indicative of low performance of the scoring system adopted by the tool  
85 (false positive variants reported with high score). **(b)** Precision/recall curves for somatic indels called by Lancet,  
86 MuTect2, LoFreq, Strelka, and Strelka2 on the virtual tumor. Number of true-positive **(c)** SNVs and **(d)** indels at  
87 different variant allele fractions for each method and for the truth call set.

88 **Virtual tumors.** Using a strategy similar to the one described in the MuTect paper<sup>8</sup>, we generated  
89 virtual tumors by introducing reads that support real germline SNVs and indels in HapMap sample  
90 NA12892, from an unrelated HapMap sample NA12891, both sequenced on the Illumina HiSeq X  
91 system. Only actual sequencing data was used to spike-in somatic variants at a ladder of variant  
92 allele fractions at variable loci identified in those sample as part of the 1000 Genomes Project  
93 (**Supplementary Fig. 3** and **Online Methods**). By knowing the true somatic variants and  
94 controlling the VAF of inserted mutations, we use the virtual tumors to test the methods' ability to  
95 call somatic mutations at predefined, including very low, VAFs. Precision/recall curves of somatic  
96 variant calls, sorted by their confidence score, show that Lancet outperforms all other somatic  
97 callers analyzed in this study on this dataset, especially for indels (**Fig. 2a-b**). On this dataset,  
98 Lancet behaves close to an (ideal) variant caller that makes no errors (straight line with  
99 precision=1) demonstrating a highly reliable scoring system for both SNVs and indels. The other  
100 tools tend to either introduce errors early by assigning high scores to false positive variants or  
101 substantially worsen in precision at higher recall rates. Although the truth set contains a handful of  
102 somatic STR mutations (**Supplementary Fig. 4**), analysis of indels called by each tool shows  
103 higher false positive rate of somatic STR indels for Strelka2, LoFreq, and MuTect2 compared to  
104 Lancet and Strelka (**Supplementary Fig. 5**); interestingly, the false positive STR indels are highly  
105 discordant across callers (**Supplementary Fig. 6b**). When calling indels, Lancet and Strelka2  
106 demonstrate higher sensitivity (**Supplementary Fig. 6a**) in particular for variants with VAF < 10%  
107 (**Fig. 2d**), however Lancet loses the least amount of precision compared to the other tools (**Fig.**  
108 **2b**). All the callers show similar performance in the detection of indels with VAF>10%, with the  
109 exception of Strelka, whose sensitivity for indels is comparable to the other methods only at 20%  
110 VAF or above. Excluding LoFreq, all the tools show similar sensitivity to detect SNVs across the  
111 VAF spectrum (**Fig. 2c**), however Lancet's superior accuracy is highlighted in the precision/recall  
112 curve (**Fig. 2a**). Finally, Lancet produces by far the best overall F<sub>1</sub>-score across all the tested  
113 methods on the virtual tumor for indel calling (**Tables 1** and **2**). Lancet and Strelka2 achieve the  
114 same F<sub>1</sub>-score on SNVs calling, however Lancet generates half the number of false positives  
115 compared to Strelka2. Analysis of the reference and alternative allele counts shows great  
116 variability in the number of supporting reads for each tool, due to the different methods and filters  
117 used in selecting the reads. As expected, most false positive indels have few reads containing the  
118 alternative allele; this is largely the case for Lancet, while other tools (e.g., MuTect2) also report  
119 false positives indels with higher support for the alternative allele, indicating a problem in  
120 selecting/filtering the set of alignments that support the mutations either in the tumor or the normal

121 (Supplementary Fig. 7). Strelka has the lowest number of false positive calls but the distribution  
122 of supporting reads highlights its limited power in detecting indels with very low support.

123 **Table 1.** Somatic indel detection performance on the virtual tumor. Tools sorted in descending order of  $F_1$ -score.

	# of calls	TP	FP	FN	Recall	Precision	FDR	$F_1$ score*	Max $F_1$ score†
<b>Lancet</b>	3891	3586	305	1359	0.72	0.92	0.078	<b>0.81</b>	<b>0.81</b>
<b>Strelka2</b>	4514	3647	867	1298	<b>0.73</b>	0.81	0.192	0.77	0.78
<b>LoFreq</b>	4853	3210	1652	1744	0.64	0.66	0.340	0.65	0.67
<b>MuTect2</b>	4873	2712	2071	2233	0.54	0.56	0.432	0.55	0.58
<b>Strelka</b>	1846	1793	53	3152	0.36	<b>0.97</b>	<b>0.028</b>	0.52	0.71

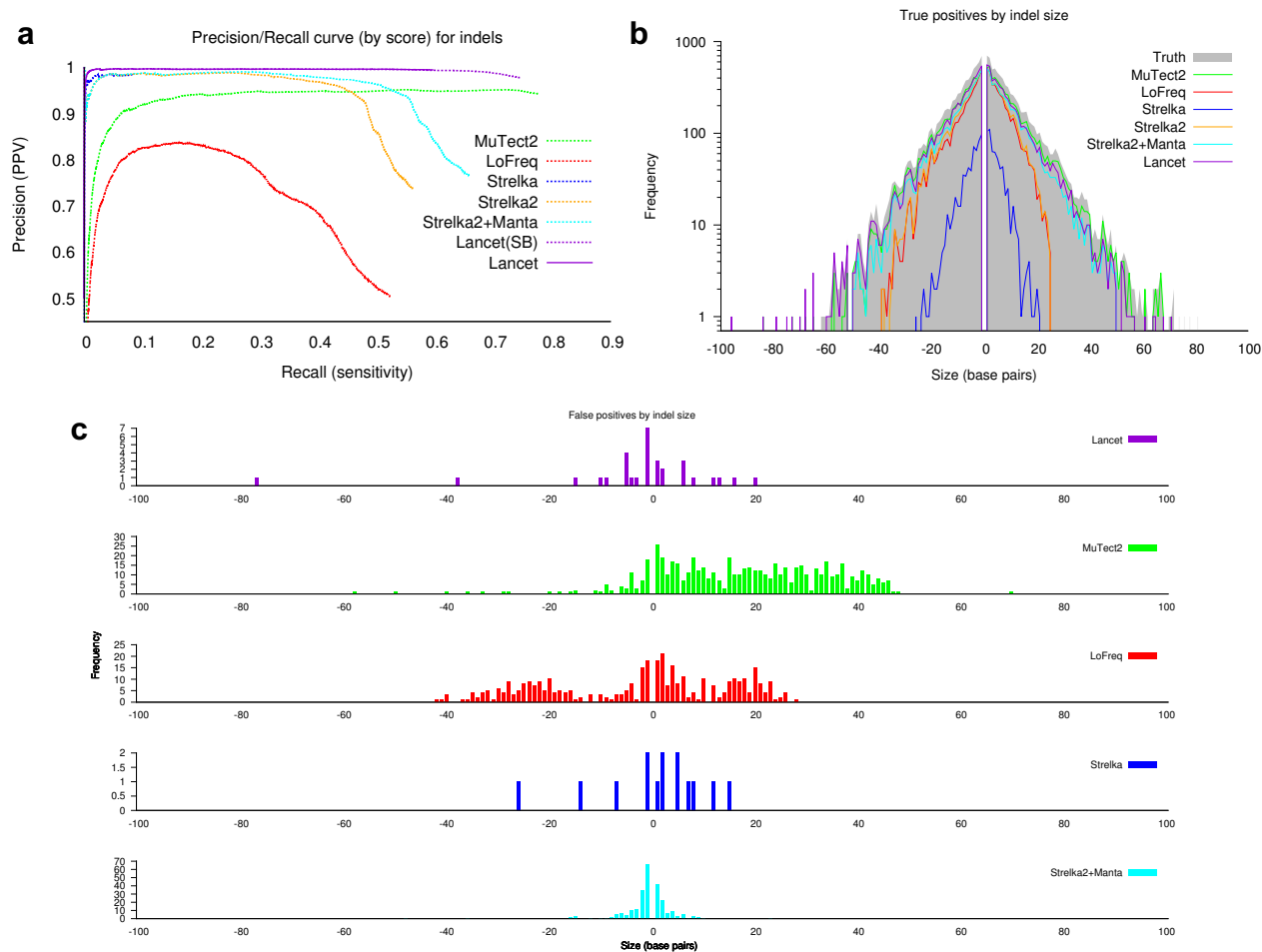
124 \*  $F_1$ score: harmonic mean of precision and recall,  $2 \times (\text{precision} \times \text{recall}) / (\text{precision} + \text{recall})$ ; † Maximum  $F_1$ score  
125 computed for each combination of precision and recall along the precision/recall curve.

126  
127 **Table 2.** Somatic SNV detection performance on the virtual tumor. Tools sorted in descending order of  $F_1$ -score.

	# of calls	TP	FP	FN	Recall	Precision	FDR	$F_1$ score*	Max $F_1$ score
<b>Lancet</b>	24413	23848	565	7744	0.75	0.98	0.023	<b>0.85</b>	<b>0.85</b>
<b>Strelka2</b>	25249	24132	1117	7460	<b>0.76</b>	0.96	0.044	<b>0.85</b>	<b>0.85</b>
<b>Strelka</b>	23891	22741	1150	8851	0.72	0.95	0.048	0.82	0.82
<b>MuTect</b>	50228	23713	2792	7879	0.75	0.89	0.055	0.82	0.82
<b>MuTect2</b>	23779	20393	3386	11199	0.65	0.86	0.142	0.74	0.74
<b>LoFreq</b>	9404	9370	34	22222	0.3	<b>0.99</b>	<b>0.003</b>	0.46	0.46

128 \*  $F_1$ score: harmonic mean of precision and recall,  $2 \times (\text{precision} \times \text{recall}) / (\text{precision} + \text{recall})$ ; † Maximum  $F_1$ score  
129 computed for each combination of precision and recall along the precision/recall curve.

130 **Synthetic tumors.** We performed an additional comparison using the synthetic tumors from the  
131 ICGC-TCGA DREAM mutation calling challenge #4. This dataset was the most difficult to  
132 analyze due to a combination of complex clonality and cellularity of the tumor sample, which  
133 contained two sub-clones of 30% and 15% allelic fraction. Similarly to the virtual tumors, raw data  
134 from a deeply sequenced sample was randomly sampled into two non-overlapping subsets of equal  
135 size. Then a spectrum of mutations, some randomly selected and some targeting known cancer-  
136 associated genes, was introduced in one of the two samples (the tumor), using BAMSurgeon  
137 (<https://github.com/adamewing/bamsurgeon>). While somatic SNVs are spiked in by altering the  
138 original reads, in the case of indels synthetic reads containing the desired mutation were simulated  
139 and used to replace a fraction of the original reads from the same region. We discovered that the  
140 truth set for this dataset contains many variants with supporting reads coming only from one strand  
141 (thus introducing a strong strand bias), and for this experiment we turned off Lancet's strand bias  
142 filter. In real tumors, such strong strand bias is unlikely to happen. Precision/recall curve analysis  
143 (**Fig. 3a**) together with the precision, FDR, and  $F_1$ -score values (**Supplementary Tables 1** and **2**)  
144 show that on this dataset Lancet outperforms all other somatic callers for indel calling. As reported  
145 in previous studies<sup>2, 15</sup>, assembly based methods, such as Lancet and MuTect2, demonstrate  
146 substantially more power to detect indels of 50 base pairs or longer compared to alignment-based  
147 methods (**Fig. 3b**). Given the longer size range of indels spiked in this dataset, we also ran Strelka2  
148 in combination with Manta<sup>16</sup>, which is the recommended protocol for best somatic indel  
149 performance. This combination is indeed more sensitive to longer indels, but it is still subject to  
150 higher error rate compared to Lancet. Analysis of the size distribution of called variants outside of  
151 STRs shows that both MuTect2 and LoFreq have strong bias towards calling longer false positive  
152 indels (**Fig. 3c**). IGV inspection of a random subset of LoFreq calls on the ICGC-TCGA DREAM  
153 data highlights that the false positive indels are typically due to mis-alignment of the supporting  
154 reads in the normal (**Supplementary Fig. 8**). Most of the MuTect2 false positive insertions instead  
155 correspond to breakpoints of larger structural variants that are misinterpreted as small insertions  
156 (**Supplementary Fig. 9-10**). For SNV detection, Lancet shows comparable results to MuTect2, the  
157 best performing method for this dataset (**Supplementary Fig. 11**). Strelka2 shows an impressive  
158 precision/recall curve for SNVs up to 0.6 recall, however its precision drops considerably  
159 afterwards.



160

161 **Figure 3. Indel performance of Lancet and other methods on the synthetic tumor #4 of the ICGC-TCGA**  
162 **DREAM mutation calling challenge.** (a) Precision/recall curve analysis of somatic indels called by Lancet, MuTect,  
163 MuTect2, LoFreq, Strelka, Strelka2, and Strelka2+Manta. Lancet<sup>SB</sup> is the version of Lancet run with strand bias filter  
164 turned off. (b) Size distribution of true positive indels for each method. Assembly based methods (Lancet, MuTect2,  
165 and Strelka2+Manta) demonstrate substantially more power to detect longer indels, while alignment-based methods  
166 (LoFreq, Strelka, and Strelka2) have reduced power to detect larger mutations, in particular insertions. (c) Size  
167 distribution of false-positive indels, excluding STRs, plotted separately for each method. LoFreq false positive indels  
168 are mostly due to mis-alignment of the reads supporting the indel in the normal, while most of the MuTect2 false  
169 positive insertions instead correspond to breakpoints of larger structural variants (e.g., inversion, translocations) that  
170 are misinterpreted as insertions. Lancet, Strelka and Strelka2 show the lowest number of false positives although  
171 Lancet has superior sensitivity compared to Strelka and Strelka2+Manta on this dataset.

172 **Normal tissue/tumor pair.** We next analyzed real data from a case of medulloblastoma used in  
173 the cross-centers benchmarking exercise of the International Cancer Genome Consortium  
174 (ICGC)<sup>13</sup>. Unlike the synthetic tumors of the ICGC-TCGA DREAM mutation calling challenge, no  
175 single mutation was spiked-in, but rather a curated list of somatic mutations (SNVs and indels) was  
176 compiled (the Gold Set). Due to the heterogeneity of the raw data (multiple library protocols,  
177 Illumina sequencers, read lengths, and fragment sizes), this dataset is particularly noisy and  
178 challenging to analyze. Moreover, differently from the previous datasets used in this study, the  
179 majority of indel calls contained in the Gold Set are located within STRs (**Supplementary Fig.**

180 **13a).** Variant calling accuracy of all tools is generally inferior in comparison to the previous  
181 benchmarking experiments (**Supplementary Fig. 12**) but final precision and recall values are in  
182 agreement with the results reported by the ICGC benchmarking team. Strelka2 and LoFreq have  
183 better precision/recall curves for indels up to 0.5 recall, but Lancet shows the best final trade-off  
184 between precision and recall ( $F_1$ -score) and it ranks second in SNV detection, after LoFreq  
185 (**Supplementary Tables 3 and 4**). Although LoFreq and Strelka2 have higher indel recall rates  
186 (**Supplementary Tables 3 and Supplementary Fig. 13b**), their final precision is substantially  
187 lower compared to Lancet and Strelka (**Supplementary Fig. 13c**), indicating that these tools may  
188 have difficulties in handling the noise in the data. Inspection of the  $F_1$ -score values, as a function of  
189 recall, shows all callers favor sensitivity over specificity in this dataset (**Supplementary Fig. 14**) –  
190 indicating that they have likely been optimized for higher quality data. As is the case with virtual  
191 tumors, false positive indels within STRs are highly discordant across callers in the  
192 medulloblastoma dataset (**Supplementary Fig. 13c-d**), thus confirming an overall lower quality of  
193 these calls. In contrast, Lancet reports a very small number of false positive indels without losing  
194 sensitivity (**Supplementary Fig. 13b-c**).

195 **Normal tissue/primary tumor/metastasis trio.** Finally, we analyzed a pair of highly genetically  
196 concordant primary and metastatic cancer lesions to check the robustness of different methods to  
197 identify shared and private somatic mutations. Concordance of SNVs shared between the primary  
198 and metastasis is much higher compared to indels among the analyzed tools, however higher  
199 agreement of the called indels is achieved when indels within STRs are removed (**Supplementary**  
200 **Fig. 15**). These results once more highlight the problem of detecting somatic STRs and emphasize  
201 the challenging, but necessary, task of integrating indel calls across different methods.

## 202 Discussion

203 Across the four datasets analyzed in this study, we discovered that the major source of  
204 disagreement between callers originates from somatic variants called within STRs, in particular if  
205 the motif is two base pairs or longer. Moreover, Venn diagram analysis shows substantial  
206 disagreement between the callers for the false positive somatic STR calls. Since the virtual tumors  
207 were created by partitioning the raw reads from a single real sample, we infer that the erroneous  
208 STR indels are the results of higher replication slippage at those sites that most tools misclassify as  
209 somatic events. In contrast, thanks to reliable scoring and filtering systems and the employment of  
210 the local assembly engine, Lancet makes fewer errors at STR sites. Alignment based tools, such as  
211 LoFreq, are inherently more prone to misclassify longer variants as somatic. Lancet instead  
212 natively corrects for mis-aligned reads thanks to the joint assembly of the tumor and normal reads  
213 in the same colored DeBruijn data structure, which also provides more precise estimation of the

214 variant allele fraction. Our extensive comparative analysis also indicates that somatic callers are  
215 now optimized for higher quality data, although inspection of the max  $F_1$ -score values suggests that  
216 better performance is achievable on noisy data with more stringent quality cutoffs.

217 The key novel feature introduced by Lancet is the usage of colored DeBruijn graphs to jointly  
218 analyze tumor and normal reads. This strategy substantially increases the accuracy of identifying  
219 mutations, especially indels, private to the tumor. Precision/recall curve analysis demonstrates that  
220 Lancet has a reliable variant quality scoring system, which is critical for prioritizing somatic  
221 variants. Lancet shows high precision when calling somatic mutations and provides robust calls  
222 across data generated by different Illumina sequencers. Due to its pure local-assembly strategy,  
223 Lancet currently has longer runtimes compared to alignment based methods (**Supplementary**  
224 **Table 5**), which is an area we plan to improve upon in the future releases of the tool. In addition to  
225 being used as a genome-wide analysis tool, Lancet can be used interactively to call variants and  
226 render colored DeBruijn graphs at small genomic regions of interest. In summary, Lancet provides  
227 highly accurate genome-wide somatic variant calling of SNVs and indels, and, given all its new  
228 features, we anticipate Lancet to become an invaluable resource for the bioinformatics community  
229 working on cancer.

## 230 Methods

231 **Lancet workflow.** Lancet uses the same local assembly engine initially developed for the Scalpel  
232 variant caller<sup>2</sup> but it introduces many new features specifically designed for somatic analysis of  
233 tumor and matched normal next-generation sequencing data. The algorithm starts by decomposing  
234 the whole genome into overlapping windows of a few hundred base pairs (600bp by default). Each  
235 region is then locally assembled, except repetitive regions that have an excessive number of  
236 mapped reads (default 10,000), using the workflow depicted in **Supplementary Fig. 1**. Reads  
237 mapping within each region are extracted from the tumor and normal BAM files and decomposed  
238 into  $k$ -mers which are then used to build a colored DeBruijn graph as described in section “Colored  
239 DeBruijn graph construction”. Reads used for the assembly are carefully selected to reduce the  
240 number of possible artifacts in the graph that could confound variant detection. The details of the  
241 read selection process and the various filters applied are described in section “Read selection”. The  
242 graph is initially built using a small  $k$ -mer value (starting with a default of  $k = 11$ ) which allows  
243 incorporation of reads supporting very low coverage variants. However, the  $k$ -mer parameter is  
244 automatically increased along the scale of odd numbers, to avoid the presence of perfect and near-  
245 perfect repeats (default up to 2 mismatches) in the graph that can confound variant detection by  
246 introducing false bubbles, described in section “Repeat analysis”. The graph complexity is then  
247 reduced by removing low-coverage nodes, dead-ends, short-links, and by compressing chains of

248 uniquely linked nodes (section “Graph cleanup”). Once a repeat-free graph has been constructed, it  
249 is anchored to the reference by selecting one *source* and one *sink* node corresponding to unique  $k$ -  
250 mers located within the current window. All possible *source-to-sink* paths are then efficiently  
251 enumerated using an Edmonds–Karp style algorithm described in section “Paths enumeration”.  
252 The assembled sequences from each path are aligned to the reference window using a sensitive  
253 Smith-Waterman-Gotoh alignment algorithm with affine-gap penalties. Finally, the alignments are  
254 parsed to extract the signature of different mutations (single nucleotide variant, insertion, and  
255 deletion).

256 **Read selection.** Reads aligning to the genome are extracted from the tumor and normal BAM files  
257 and used for local assembly with the exception of the following set of reads. (1) PCR duplicates  
258 marked using the Picard MarkDuplicates module (<https://broadinstitute.github.io/picard>) –  
259 removing PCR duplicates is necessary to correctly estimate coverage and support for variant calls.  
260 (2) Reads aligned with low mapping quality (< MP, default 15) – reads with low mapping quality  
261 may be mapped to the wrong genomic location or aligned with incorrect signature. (3) Reads  
262 which are highly likely to be multi-mapped. Depending on which version of the BWA aligner is  
263 employed, there are two ways to identify these reads. In the case of BWA-MEM, multi-mapped  
264 reads are assigned equal values in the AS and XS tags, however we slightly relaxed this constraint  
265 to identify reads which are highly likely to be multi-mapped ( $|AS-XS| \leq \delta$  where  $\delta = 5$ ). If BWA-  
266 ALN is employed, multi-mapped reads are marked using the XT:Z::R tag, nonetheless, their  
267 mapping quality is not necessarily zero. This is because mapping quality is computed for the read  
268 pair, while XT is only determined from a single read. For example, when the mate of a read can be  
269 mapped unambiguously, the read can still be mapped confidently and thus assigned a high  
270 mapping quality. In addition to the XT tag, multi-mapped reads are also identified using the XA  
271 tag which is used to list the alternative hits of the read across the genome. Finally, to maximize the  
272 sensitivity to detect variants that are also present in the normal sample, no filter is applied when  
273 extracting the reads aligned to the normal.

274 **Colored DeBruijn graph construction.** The key data structure used by Lancet is the colored  
275 DeBruijn graph constructed using the reads from both the tumor and the matched normal samples.  
276 **Fig. 1** shows an example of the DeBruijn graphs generated by Lancet. Formally the graph is  
277 defined as  $G(V, E, C)$  where  $V$  is the set of vertices/nodes corresponding to the different  $k$ -mers  
278 extracted from the reads,  $E$  is the set of edges connecting two nodes having a  $k-1$  perfect match  
279 between their respective  $k$ -mers, and  $C$  is the coloring scheme (labels) used to indicate whether the  
280  $k$ -mer has been extracted from the tumor or normal sample. To account for the double-strandedness  
281 of DNA, Lancet constructs a bi-directed DeBruijn graph where each node stores both forward and  
282 reverse complement of each  $k$ -mer. The graph is augmented with ancillary information extracted

283 from the raw sequencing data, specifically each node stores (i) the  $k$ -mer counts split by strand, (ii)  
284 the list of reads where the  $k$ -mers were found, and (iii) the Phred quality for each base. The  $k$ -mers  
285 from the reference sequence are also extracted and incorporated into the graph. Sequencing data is  
286 typically generated from short-insert paired-end DNA libraries and the variable fragment size  
287 distribution can sometimes cause two paired reads to overlap each other. Therefore, coverage  
288 needs to be adjusted to avoid over counting the overlapping portion of the two reads. This is easily  
289 accomplished in the DeBruijn graph framework since  $k$ -mers extracted from the overlapping  
290 segment come from reads that share the same query template (QNAME) in the BAM file. If this  
291 condition is detected, the  $k$ -mer count is adjusted to only count one copy of the two  $k$ -mers.

292 **Graph cleanup.** Sequencing errors, coverage fluctuations, and mapping errors increase the graph  
293 complexity by introducing nodes and edges that confound the analysis. Lancet utilizes several  
294 graph operations and transformations designed to remove spurious nodes and edges introduced  
295 during graph construction. First, low-coverage nodes, which are typically associated with  
296 sequencing errors, are removed if the corresponding  $k$ -mer count is below a specific user defined  
297 threshold (default 1) or if the coverage ratio is below a certain user defined value (default 0.01).  
298 Second, dead-ends are removed, which present themselves as a sequence of uniquely linked nodes  
299 that do not connect back to the graph (also called short tips). Dead-ends formed by  $n$  (default 11)  
300 or more nodes are removed from the graph. Next *short-links* are removed, which are short  
301 connections composed by fewer nodes than theoretically possible given the  $k$ -mer value used to  
302 build the graph. **Supplementary Figure 16** illustrates one exemplary short-link scenario. This type  
303 of connection is typically due to sequence homology between closely located repeats (e.g., Alu  
304 repeats), but it can also happen in the case of long homopolymers, and other short tandem repeats,  
305 where the tandem repetition of the motif can result in the construction of a tiny bubble in the  
306 presence of a heterozygous mutation. Those tiny bubbles need to be kept in the graph as they may  
307 represent true variation, while short-links like the one depicted in **Supplementary Fig. 18** can be  
308 safely removed. Therefore, connections at non-STR sites formed by  $m$  ( $\ll k$ ) or less nodes and  
309 whose minimum coverage node is  $c < \sqrt{c_{avg}}$  are removed from the graph, where  $c_{avg}$  is the average  
310 coverage across the window. Finally, the graph is compressed by merging chains of uniquely  
311 linked nodes into super nodes.

312 **Repeat analysis.** Small scale repeats are a major challenge for accurate variant calling, specifically  
313 for indels<sup>1</sup>. To avoid introducing errors at those loci, Lancet employs the same repeat analysis  
314 procedure introduced in the Scalpel algorithm. Specifically, the sequence composition in each  
315 window is analyzed for the presence of perfect or near-perfect repeats (up to a specified number of  
316 mismatches, 2 by default) of size  $k$ . Similarly, the graph is inspected for the presence of cycles  
317 (perfect repeats) or near-perfect repeats in any of the source-to-sink paths. If a repeat structure is

318 detected, a larger  $k$ -mer value is selected and the repeat analysis is performed again on both the  
319 reference sequence and the newly constructed graph, until a repeat-free graph is constructed or the  
320  $k$ -mer size has reached a maximum value (101 by default). To avoid using  $k$ -mers which are  
321 reverse complement of their own sequences, only odd values of  $k$  are used to build the graph. This  
322 iterative strategy is a key feature of the Lancet algorithm which automatically selects the optimal  $k$ -  
323 mer size according to the sequence composition of each genomic window.

324 **Paths enumeration.** Enumerating all possible haplotypes can take time, growing exponentially  
325 with the number of bubbles present in the graph. To reduce the computational requirements of the  
326 graph traversal down to polynomial time, we employ an Edmonds–Karp style algorithm for fast  
327 enumeration of all possible haplotypes. The idea behind the algorithm is to find the minimum  
328 number of paths from source to sink that cover every edge in the graph (edge and nodes can be  
329 visited more than once). The pseudo code of the algorithm is presented below. Since every node is  
330 visited (possibly multiple times), it is easy to show that, although the same variant could be  
331 discovered multiple times, no variant is missed from the analysis. Straightforward complexity  
332 analysis of the pseudocode shows that the worst-case time complexity is  $O(E^2+EV)$ : at least one  
333 edge is visited at each iteration (step 5) accounting for  $O(E)$  time, and each call to the graph  
334 traversal (step 2) takes  $O(E+V)$  where  $E$  is the number of edges and  $V$  the number of nodes in the  
335 graph. As such, a trivial upper bound for the whole procedure is  $O(E) \times O(E+V) = O(E^2+EV)$ .

336 1. **while** (*true*) {  
337 2.     path = bfs(*source*, *sink*, *dir*, *ref*); /\* with at least one unvisited edge \*/  
338 3.     **if** (*path* == *null*) { **break**; }  
339 4.     processPath(*path*); /\* align sequence to reference and extract variants \*/  
340 5.     **for each** edge in *path* {  
341 6.         *Edge.visited* = *true*;  
342 7.     }  
343 8. }  
344

345 **Active regions.** The idea behind the active region module is to avoid wasting time processing (read  
346 extraction, local assembly, re-alignment) regions without evidence for variation. Regions where all  
347 reads map to the reference without any mismatches can be trivially discarded. However, the error  
348 rate of the Illumina sequencing technology (~0.1 percent), in combination with high coverage,  
349 makes the scenario of alignments with no mismatches in a region very unlikely. The policy  
350 adopted by Lancet is to consider a region as “active”, either in the tumor or the normal sample, if a  
351 minimum of  $N$  (aligned) reads support a mismatch, indel, or soft-clipped sequence at the same  
352 locus (**Supplementary Fig. 17**), where  $N$  is equal to the minimum alternative count support

353 specified for somatic variants (3 by default). This policy is implemented on the fly by simple and  
354 fast parsing of the MD and CIGAR strings. This step is functionally similar to the active region  
355 module employed in MuTect and other tools, however Lancet follows a pure assembly approach,  
356 where all variant types (SNVs, insertions and deletions) are detected through local assembly. When  
357 tested on an 80x/40x coverage pair of tumor/normal samples sequenced with 150bp reads, Lancet's  
358 active region strategy discards on average between ~10% and ~20% of the total number of  
359 windows. However, due to its pure assembly strategy, Lancet typically requires higher runtimes  
360 compared to the hybrid approach employed by MuTect2 and Strelka2 (**Supplementary Table 5**).  
361 To achieve faster runtimes and to discard more windows, the parameter  $N$  can be increased when  
362 analyzing samples sequenced at coverage higher than 80x/40x.

363 **Scoring variants.** Fisher's Exact test is used to determine if a mutation has non-random  
364 associations between the allele counts in the tumor and in the normal samples. Specifically, given a  
365 somatic mutation, reference and alternative reads supporting the variant both in the tumor and the  
366 normal are collected and stored into a 2-by-2 contingency table which is then used to compute a  
367 Phred-scaled Fisher's exact test score,  $S_{(fet)}$ , according to the following formula:

$$S_{(fet)} = \begin{cases} 0 & \text{if } p == 1 \\ -10\log_{10}(p) & \text{otherwise} \end{cases}$$

369 where  $p$  is the exact probability of the 2-by-2 contingency table given by the hypergeometric  
370 distribution.

371 **Variant filters.** Lancet generates the list of mutations in VCF format<sup>17</sup> (v4.1). All variants (SNVs  
372 and indels) either shared, specific to the tumor, or specific to the normal are exported as part of the  
373 output. Following the VCF format best practices, high quality variants are labelled as PASS in the  
374 FILTER column. Several standard filters, all of which have tunable parameters, are applied to  
375 remove germline calls and low quality somatic variants as describe here:

- 376 1. *Low/high coverage:* mutations located in substantially low coverage regions of the normal  
377 (default < 10) or tumor (default < 4) are removed since there is a high chance for coverage  
378 bias towards one of the alleles.
- 379 2. *Variant allele fraction:* mutations characterized by a very low variant allele fraction in the  
380 tumor (default < 0.04) are filtered because they are likely to be false positive calls.  
381 Likewise, variants whose variant allele fraction is high in the normal (default > 0.0) are  
382 considered to be germline calls.

383 3. *Alternative allele count*: analogously to the allele fraction filter, mutations with low  
384 alternative allele count (default < 3) in the tumor are likely to be false positive calls and are  
385 flagged as low quality. While variants with a high alternative allele count in the normal  
386 (default > 0) are considered to be germline mutations.

387 4. *Fisher's exact test (FET) score*: mutations with a very low FET score are flagged as low  
388 quality. Due to their inherently different error profiles, separate thresholds are used for non-  
389 STR variants (default < 5.0) and STR variants (default < 25.0).

390 5. *Strand bias*: this filter rejects variants where the number of alternative counts in the forward  
391 or reverse strand is below a certain threshold (default < 1).

392 6. *Microsatellite*: microsatellites (or short tandem repeats) are highly mutable genetic  
393 elements subject to high rate of replication slippage events (especially homopolymers),  
394 which reduces variant callers' ability to distinguish between sequencing errors and true  
395 mutations. As such, mutations located within microsatellites or in their proximity (default 1  
396 base pair away) are recognized and flagged by Lancet. By default, microsatellites are  
397 defined as sequences composed of at least 7bp (total length), where the repeat sequence is  
398 between 1bp and 4bp, and is repeated at least 3 times. The user can adjust these parameters  
399 to define any type of microsatellite motif size and length as required by different  
400 applications.

401 **Read alignment and BAM file generation.** Sequencing reads were aligned to the human  
402 reference hg19 using BWA-MEM (v.0.7.8-r455) with default parameters. Alignments were  
403 converted from SAM format to sorted and indexed BAM files with SAMtools (v.1.1). GATK  
404 software tools (v.2.7-4) were used for improving alignments around indels (GATK IndelRealigner)  
405 and base quality recalibration (GATK base quality recalibration tool) using recommended  
406 parameters. Finally, the Picard tool set (v.1.119) was used to remove duplicate reads. The final  
407 BAM files generated by this process were used as input for all the variant callers used in this study.

408 **Virtual tumors.** We created virtual tumors using a strategy similar to what was employed in the  
409 MuTect paper<sup>8</sup>. We sequenced HapMap sample NA12892 at high coverage on the Illumina HiSeq  
410 X system using PCR-free protocol and partitioned the set of reads into two groups of 80x and 40x  
411 average coverage to use as tumor and normal respectively. Reads were mapped using the  
412 alignment procedure described in section “Read alignment and BAM file generation”. We then  
413 used an unrelated HapMap sample NA12891 sequenced on the same Illumina HiSeq X system to  
414 introduce realistic SNVs and indels by swapping a predefined number of reads between the two  
415 samples at loci where NA12892 is homozygous reference and NA12891 is homozygous variant

416 (Supplementary Fig. 3). The list of selected loci is based on the 1000 Genomes Project phase 3<sup>18</sup>  
417 call set and the number  $N$  of reads that were swapped between the two samples followed a  
418 binomial distribution with mean  $\mu = 0.05, 0.1, 0.2, 0.3$ . This procedure allowed us to spike-in  
419 realistic mutations with known variant allele fractions, but the length of indels was limited by the  
420 short size range currently included in the 1000 Genomes call set. Specifically, the longest insertion  
421 and deletions that we were able to spike in were 13 bp and 35 bp respectively. We used this  
422 process separately for SNVs and indels to create two pairs of tumor/normal samples with 31,592  
423 somatic SNVs and 4,945 somatic indels respectively. The virtual tumor BAM files together with  
424 the list of true variants are freely available for download at the New York Genome Center ftp site  
425 (<ftp://ftp.nygenome.org/lancet>).

426 **ICGC medulloblastoma benchmarking data.** We downloaded the full set of FastQ files of the  
427 medulloblastoma patient (accession number EGAD00001001859) from the European Genome-  
428 phenome Archive (EGA, <https://www.ebi.ac.uk/ega>). The raw reads were generated by five  
429 different sequencing centers reaching a cumulative coverage of ~300X for both the tumor and the  
430 normal samples. We merged the raw FastQ files separately for the tumor and the normal samples  
431 and then aligned the reads using the alignment pipeline described in section “Read alignment and  
432 BAM file generation”. Then we down-sampled the ~300X BAM files down to ~80X and ~40x for  
433 the tumor and the normal respectively using the Picard DownsampleSam module. The down-  
434 sampled BAM files generated by this process were then used as input for all the somatic variant  
435 callers used in this study.

436 **Primary and metastatic cancer lesions data.** Sequencing data for the paired primary and  
437 metastatic cancer lesions are publicly available through the database of Genotypes and  
438 Phenotypes (dbGaP, <https://www.ncbi.nlm.nih.gov/gap>) with accession number phs000790.v1.p1.  
439 The same data is also available through the Memorial Sloan Kettering Cancer Center cBioPortal  
440 for Cancer Genomics (study “Colorectal Adenocarcinoma Triplets”). In this study, we used the  
441 sequencing data for sample EV-014 and the BAM files were created following the same procedure  
442 described in section “Read alignment and BAM file generation”, with the only difference that the  
443 normal, primary and metastatic samples have been realigned together (with GATK IndelRealigner)  
444 to further improve alignments around indels.

445 **Variant calling.** We tested the variant calling abilities of eight different somatic variant callers:  
446 Lancet (v1.0.0), MuTect (v1.1.7), MuTect2 (v2.3.5), LoFreq (v2.1.2), Strelka (v1.0.14), Strelka2  
447 (v2.8.3), Scalpel<sup>2</sup> (v0.5.3), and VarDict<sup>19</sup> (v328e00a). Although a larger number of somatic variant  
448 callers is available in the literature, we chose to compare Lancet against these methods because  
449 they are some of the most widely used approaches specifically designed for whole genome  
450 tumor/normal variant calling and they represent a combination of both assembly and alignment

451 based methods. Default parameters were used for each tool. Results on the virtual tumors revealed  
452 Scalpel and VarDict to be outliers in terms of specificity (**Supplementary Fig. 18**), so we decided  
453 to exclude these two tools from the overall benchmarking experiments.

454 **Benchmarking workflow.** We used the following procedure to perform the Precision/Recall curve  
455 analysis employed in this study:

- 456 1. First, we ran each tool with default parameters, as reported in the “Variant calling” section.
- 457 2. We kept only the PASS somatic variants within the autosomes together with chromosomes  
458 X, Y and sorted the variant calls, from highest quality to the lowest, according to the  
459 quality score reported by each method in the final VCF file (“FisherScore” for Lancet,  
460 “SomaticEVS” for Strelka2, “QSI” for Strelka, “QUAL” for LoFreq, “TLOD” for MuTect  
461 and MuTect2).
- 462 3. Due to the possibly ambiguous representation of indels around microsatellites and other  
463 simple repeats, we left normalized all the indels.
- 464 4. When comparing calls to the truth set or across the different methods, we matched two  
465 variants (SNV or indels) if they shared the same genomic coordinates (chromosome and  
466 start position) as well as if they have the exact same sequences (both in size and base pair  
467 composition) in the reference and alternative alleles.
- 468 5. Precision/recall values along the curve are then computed for each tool by processing the  
469 somatic calls in the sorted order generated in step 2.

470 **Code availability and system requirements.** Lancet is written in C/C++ and is freely available  
471 for academic and non-commercial research purposes as an open-source software project at  
472 <https://github.com/nygenome/lancet>. Lancet employs two widely used next-generations sequencing  
473 analysis APIs/libraries, BamTools (<https://github.com/pezmaster31/bamtools>) and HTSlib  
474 (<http://www.htslib.org/>), to read and parse the information in the BAM file, which are included in  
475 the code distribution. The source code has no dependencies and it is easy to compile and runs  
476 across different operating systems (Linux and Mac OSX). Lancet supports native multithreading  
477 via pthreads parallelization. Analysis of one whole-genome (80x/40x) tumor-normal pair  
478 sequenced with 150 base pair reads usually requires 3000 core hours and a minimum of 20 GB of  
479 RAM on a modern machine after splitting the analysis by chromosome.

480 **Data availability.** Data used in this study was retrieved from the 1,000 Genomes website  
481 (<http://www.1000genomes.org>), the European Genome-phenome Archive (EGA,  
482 <https://www.ebi.ac.uk/ega> with accession number EGAD00001001859, the database of Genotypes  
483 and Phenotypes (dbGaP, <https://www.ncbi.nlm.nih.gov/gap>) with accession number  
484 phs000790.v1.p1, and the International Cancer Genome Consortium (ICGC, <http://icgc.org/>). The

485 virtual tumors generated and analyzed in this study are freely available for download at the New  
486 York Genome Center public ftp site (<ftp://ftp.nygenome.org/lancet>).

## 487 Acknowledgments

488 We thank Michael C. Schatz and Wayne Clarke for the helpful discussion and comments on the  
489 manuscript.

## 490 Authors contributions

491 G.N. designed the algorithms, developed the software, and conducted the computational  
492 experiments. A.C., A.K.E., V.V., M.Z. contributed to the design of algorithms. K.A., E.A.B., M.S.,  
493 assisted with benchmarking the different somatic variant caller. R.M. assisted with the integration  
494 of multiple high-throughput sequencing APIs. All authors assisted with the design and  
495 interpretation of the comparative analysis between the different methods. G.N. wrote the  
496 manuscript with input from all the authors. All of the authors have read and approved the final  
497 manuscript.

498 **Competing Financial Interests.** The authors declare no competing financial interests.

## 499 References

- 500 1. Narzisi G, Schatz MC. The challenge of small-scale repeats for indel discovery. *Front  
501 Bioeng Biotechnol* **3**, 8 (2015).
- 502 2. Narzisi G, *et al.* Accurate de novo and transmitted indel detection in exome-capture data  
503 using microassembly. *Nat Methods* **11**, 1033-1036 (2014).
- 505 3. Iqbal Z, Caccamo M, Turner I, Flicek P, McVean G. De novo assembly and genotyping of  
506 variants using colored de Bruijn graphs. *Nat Genet* **44**, 226-232 (2012).
- 508 4. Li H, *et al.* The Sequence Alignment/Map format and SAMtools. *Bioinformatics* **25**, 2078-  
509 2079 (2009).
- 511 5. Barnett DW, Garrison EK, Quinlan AR, Stromberg MP, Marth GT. BamTools: a C++ API  
512 and toolkit for analyzing and managing BAM files. *Bioinformatics* **27**, 1691-1692 (2011).

514

515 6. Quinlan AR, Hall IM. BEDTools: a flexible suite of utilities for comparing genomic  
516 features. *Bioinformatics* **26**, 841-842 (2010).

517 7. Robinson JT, *et al.* Integrative genomics viewer. *Nat Biotechnol* **29**, 24-26 (2011).

519 8. Cibulskis K, *et al.* Sensitive detection of somatic point mutations in impure and  
520 heterogeneous cancer samples. *Nat Biotechnol* **31**, 213-219 (2013).

522 9. Wilm A, *et al.* LoFreq: a sequence-quality aware, ultra-sensitive variant caller for  
523 uncovering cell-population heterogeneity from high-throughput sequencing datasets.  
524 *Nucleic Acids Res* **40**, 11189-11201 (2012).

526 10. Saunders CT, Wong WS, Swamy S, Becq J, Murray LJ, Cheetham RK. Strelka: accurate  
527 somatic small-variant calling from sequenced tumor-normal sample pairs. *Bioinformatics*  
528 **28**, 1811-1817 (2012).

530 11. Sangtae Kim KS, Aaron L Halpern, Mitchell A Bekritsky, Eunho Noh, Morten Källberg,  
531 Xiaoyu Chen, Doruk Beyter, Peter Krusche, Christopher T Saunders. Strelka2: Fast and  
532 accurate variant calling for clinical sequencing applications. *bioRxiv*, (2017).

534 12. Ewing AD, *et al.* Combining tumor genome simulation with crowdsourcing to benchmark  
535 somatic single-nucleotide-variant detection. *Nat Methods* **12**, 623-630 (2015).

537 13. Alioto TS, *et al.* A comprehensive assessment of somatic mutation detection in cancer  
538 using whole-genome sequencing. *Nat Commun* **6**, 10001 (2015).

540 14. Brannon AR, *et al.* Comparative sequencing analysis reveals high genomic concordance  
541 between matched primary and metastatic colorectal cancer lesions. *Genome Biol* **15**, 454  
542 (2014).

544 15. Rimmer A, *et al.* Integrating mapping-, assembly- and haplotype-based approaches for  
545 calling variants in clinical sequencing applications. *Nat Genet* **46**, 912-918 (2014).

547 16. Chen X, *et al.* Manta: rapid detection of structural variants and indels for germline and  
548 cancer sequencing applications. *Bioinformatics* **32**, 1220-1222 (2016).

550 17. Danecek P, *et al.* The variant call format and VCFtools. *Bioinformatics* **27**, 2156-2158  
551 (2011).

553

554 18. Genomes Project C, *et al.* A global reference for human genetic variation. *Nature* **526**, 68-

555 74 (2015).

556

557 19. Lai Z, *et al.* VarDict: a novel and versatile variant caller for next-generation sequencing in

558 cancer research. *Nucleic Acids Res* **44**, e108 (2016).

559

560